

Review

The Role of Reductive Carbonaceous Surrounding Rocks in the Formation of Porphyry Mo Deposits

Dongwei Guo ^{1,2}, Yanhe Li ^{1,*}, Chao Duan ^{1,*}, Changfu Fan ¹ and Pengcheng Sun ¹

¹ Ministry of Natural Resources Key Laboratory of Metallogeny and Mineral Assessment, Institute of Mineral Resources, Chinese Academy of Geological Sciences, Beijing 100037, China; guodongwei@stu.pku.edu.cn (D.G.); tjfchangfu@163.com (C.F.); pengchengsun1225@163.com (P.S.)

² School of Earth and Space Sciences, Peking University, Beijing 100871, China

* Correspondence: lyh@cei.cn (Y.L.); duanchao@cags.ac.cn (C.D.)

Abstract: Porphyry Mo deposits are the most important type of Mo resource. They result from a high oxygen fugacity of the parent magma, which acts as an effective indicator for evaluating the mineralization. In the ore-forming system of porphyry Mo deposits, sulfur exists mainly as sulfate in highly oxidized magma but as sulfide in ores. What triggers the reduction in the mineralization system that leads to sulfide precipitation has not yet been determined. Most of the previous studies have focused on the origin and evolution of the ore-forming parent magma, and the effects of reductive surrounding rocks on porphyry mineralization have been ignored. In this study, a comprehensive geological–geochemical investigation and review have been performed on the typical porphyry Mo deposits, the Nannihu-Sandaozhuang, Yuchiling, and Shapingou deposits in China, and the Mt. Emmons deposits in America. Black carbonaceous sedimentary layers commonly surround porphyry Mo ores, which are widely altered and discolored during mineralization. CH₄ is commonly present in fluid inclusions in the main mineralization stage, and the $\delta^{13}\text{C}_{\text{V-PDB}}$ values of calcite and fluid inclusions from the altered surrounding rocks and ore minerals are generally low and significantly different from those of marine sedimentary carbonate rocks, indicating that the involvement of reductive components from carbonaceous surrounding rocks might be key to the redox state transformation leading to mineral precipitation. On the other hand, the CH₄ produced by the thermal decomposition of organic matter or carbonaceous reaction with H₂O can diffuse into the ore-forming system along the structural fractures and reduce the SO₄²⁻ in the ore-forming hydrothermal fluids to form sulfide precipitation without direct contact between the intrusion and the carbonaceous surrounding rocks. Moreover, the CH₄ content controls the location of the orebody formation with the high content producing orebodies mainly in the porphyry intrusion, while the low CH₄ content results in the orebodies mainly occurring at the contact zone between the porphyry and carbonaceous surrounding rocks. Compared to the magmatic stage of mineralization, the involvement of reductive components in the carbonaceous surrounding rocks during the hydrothermal stage is more favorable for forming giant/large Mo deposits. The highly oxidized porphyry with reductive carbonaceous surrounding rocks or Fe-rich volcanic rocks offers a new indicator for efficiently evaluating porphyry Mo mineralization.

Keywords: porphyry Mo deposits; high oxygen fugacity; redox state transformation; carbonaceous surrounding rocks; reductive agent CH₄



Citation: Guo, D.; Li, Y.; Duan, C.; Fan, C.; Sun, P. The Role of Reductive Carbonaceous Surrounding Rocks in the Formation of Porphyry Mo Deposits. *Minerals* **2023**, *13*, 951. <https://doi.org/10.3390/min13070951>

Academic Editor: David Lentz

Received: 24 June 2023

Revised: 13 July 2023

Accepted: 14 July 2023

Published: 17 July 2023



Copyright: © 2023 by the authors. Licensee MDPI, Basel, Switzerland. This article is an open access article distributed under the terms and conditions of the Creative Commons Attribution (CC BY) license (<https://creativecommons.org/licenses/by/4.0/>).

1. Introduction

Porphyry Mo deposits are an important source of Mo resources. The distribution of Mo resources is uneven globally, with approximately 90% of molybdenum distributed in China, America, Peru, Chile, and Canada [1]. The formation of porphyry molybdenum deposits is closely related to the subduction of the oceanic crust [2]. They have been classified as Climax-type (rift-related, represented by the deposits in the Climax-Henderson Mo belt in

America) [3–5], Endako-type (arc-related, represented by the Endako and MAX deposits in Canada; Quartz Hill, Thompson Creek, and Buckingham deposits in America; Tamboras deposit in Peru; and deposits in the Gangdese metallogenic belt and the Central Asian orogenic belt in China) [6–18], and Dabie-type (collision-related, typified by deposits in the Qingling-Dabie Mo belt in China) deposits [19–23].

The parent magma of porphyry Mo deposits often contains primitive gypsum, magnetite/hematite, and other highly oxidized minerals, implying a very high oxygen fugacity of the primitive magma [3,4,24–31]. The high oxygen fugacity of the initial magma is favorable for chalcophile ore metal elements such as Cu and Mo to enter the magma as incompatible components during partial melting, forming sulfur-rich and Mo-rich ore-forming magma. Furthermore, the high oxygen fugacity makes the sulfur present mainly as sulfate anions, which prevents ore-forming metal elements from precipitating as sulfide in the magma during the migration and evolution of magma [32–34]. Therefore, a high oxygen fugacity has become a widely accepted criterion for distinguishing mineralized and nonmineralized porphyries [34–44]. A high fractionation and oxygen fugacity of the parent magma and enrichment of Mo, S, and H₂O are favorable conditions for porphyry Mo ore production [45]. However, in some deposits, melts and fluids in mineralization systems have lower Mo contents (2–25 ppm) [30,46–48], indicating conditions for the accumulation and efficient unloading of ore-forming materials, which may be more important than the initial Mo concentration of magma [49].

Sulfur exists mainly as sulfate anions in the highly oxidized magma but also as sulfide in ores, indicating significant changes in redox conditions during mineralization. This variation is an essential scientific issue related to the genesis and efficient evaluation of porphyry Mo deposits. However, there is no specific interpretation yet. Li and his coauthors proposed that highly oxidized porphyry with reductive carbonaceous surrounding rocks or Fe-rich volcanic rocks was a new indicator for efficiently evaluating porphyry mineralization [42]. There are two primary reductive surrounding rocks related to porphyry mineralization: carbonaceous surrounding rocks and Fe-rich volcanic rocks [42]. Carbonaceous surrounding rocks are more developed in porphyry Mo deposits in China [22,50–55], and Fe-rich volcanic rocks are prevalent in porphyry Mo deposits in South America [56–59]. In this study, the Nannihu-Sandaozhuang-Shangfanggou, Shapingou, and Yuchiling giant or large porphyry Mo deposits in the eastern Qinling-Dabie Mo mineralization belt in central China and the Mt. Emmons Mo deposits in the Mo mineralization belt in Colorado in America were selected as examples; the involvement of carbonaceous surrounding rocks in the mineralization process was discussed, and a new indicator for evaluating the mineralization of porphyry Mo deposits was proposed.

2. Geological Characteristics of Porphyry Mo Deposits and Their Relationship with Carbonaceous Surrounding Rocks

Numerous studies have demonstrated that dark-black reductive carbonaceous sedimentary layers are widely developed in the roof and surrounding rocks of giant or large porphyry Mo deposits, such as the Shuidigou Formation of the Proterozoic Taihua Supergroup and the Xianrenchong Formation of the Proterozoic Luzhenguan Group, which contains graphitic schist and graphite gneiss; the Baishugou, Sanchuan, Nannihu and Meiyaogou Formations of the Neoproterozoic Luanchuan Group, which contains carbonaceous slate and shale developed in the East Qinglin-Dabie Mo mineralization belt (Figure 1) [22,50–55,60,61]; and the Cretaceous Mancos Formation and Mesaverde Group, which contains coal and carbonaceous shale and siltstone that are widely distributed in the Climax-Henderson Mo mineralization belt in North America [25,62–67]. Carbonaceous sedimentary layers provide reductive agents for the porphyry mineralization system and serve as an ideal natural water-resisting layer, critical factors, and conditions for forming high-grade porphyry Mo ores. The CH₄, produced by organic matter pyrolysis or carbonaceous interaction with hydrothermal fluids, triggers a sulfate reduction in highly oxidizing mineralization solutions and subsequent efficient ore precipitation. To further understand

the role of carbonaceous surrounding rocks in porphyry mineralization, we chose several typical Mo deposits in East Qinling-Dabie and Climax-Henderson, which are the world's two most extensive Mo mineralization belts, as shown below in Figure 1.

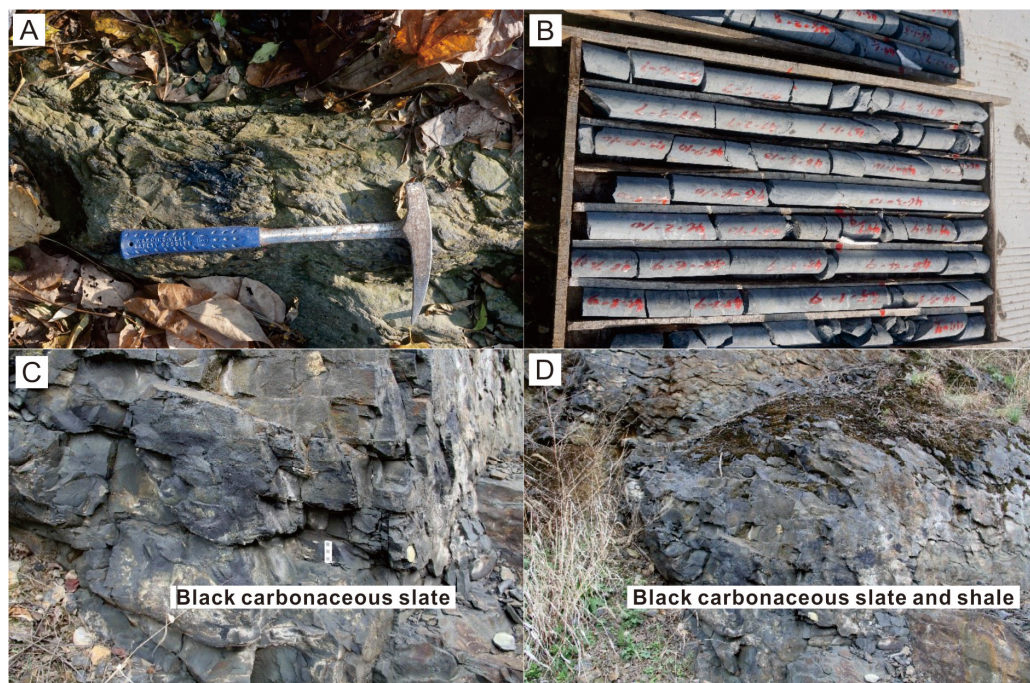


Figure 1. Carbonaceous surrounding rocks are closely related to Mo mineralization in the East Qinling-Dabie Mo mineralization belt. (A) The surface exposure of the Sanhe graphite deposit occurred in the Xianrenchong Formation of the Luzhenguan Group in the periphery of the Shapinggou Mo deposit in Jinzhai. (B) Rock cores from the Sanhe graphite deposit in Xingfu village. (C) The thick-layered black carbonaceous slate of the Baishugou Formation within the boundary of the Nannihu-Sandaozhuang Mo deposits. (D) Black carbonaceous slate and shale of the Baishugou Formation within the boundary of the Nannihu-Sandaozhuang Mo deposits.

2.1. Nannihu-Sandaozhuang-Shangfanggou Mo-(W) Porphyry-Skarn Deposits

The Luanchuan ore field, which is situated in the western part of the East Qinling-Dabie Mo mineralization belt, includes the Nannihu Mo-(W) porphyry deposit, the Sandaozhuang Mo-(W) skarn deposit, and the Shangfanggou Mo-Fe porphyry deposit (Figures 2 and 3) [50,68]. The total measured Mo reserves are more than 200×10^4 t, with a large W reserve of more than 70×10^4 t [51]. The outcropping strata consist of the Mesoproterozoic Guandaokou Group and the Neoproterozoic Luanchuan Group, comprising the Baishugou, Sanchuan, Nannihu, and Meiyaogou Formations, listed in ascending order. The Yanshanian metallogenic granite porphyry intrudes into the Nannihu Formation and the ore body occurs in the granite porphyry and altered biotite-feldspar hornfels in the Nannihu Mo-(W) porphyry deposit. Similarly, the thick-layered ore body is mainly hosted in the calc-silicate hornfels and the skarns in the upper Sanchuan Formation in the Sandaozhuang Mo-(W) skarn deposit (Figure 4). In the Shangfanggou Mo-Fe deposit, the Mo orebodies occur in the porphyritic biotite granite and its contact zones with the Meiyaogou Formation, including stone coal seams with thicknesses greater than 154 m, as well as in the altered gabbro. The layered Fe ores occur in the contact zone between the granite porphyry and the marble (Figure 5).

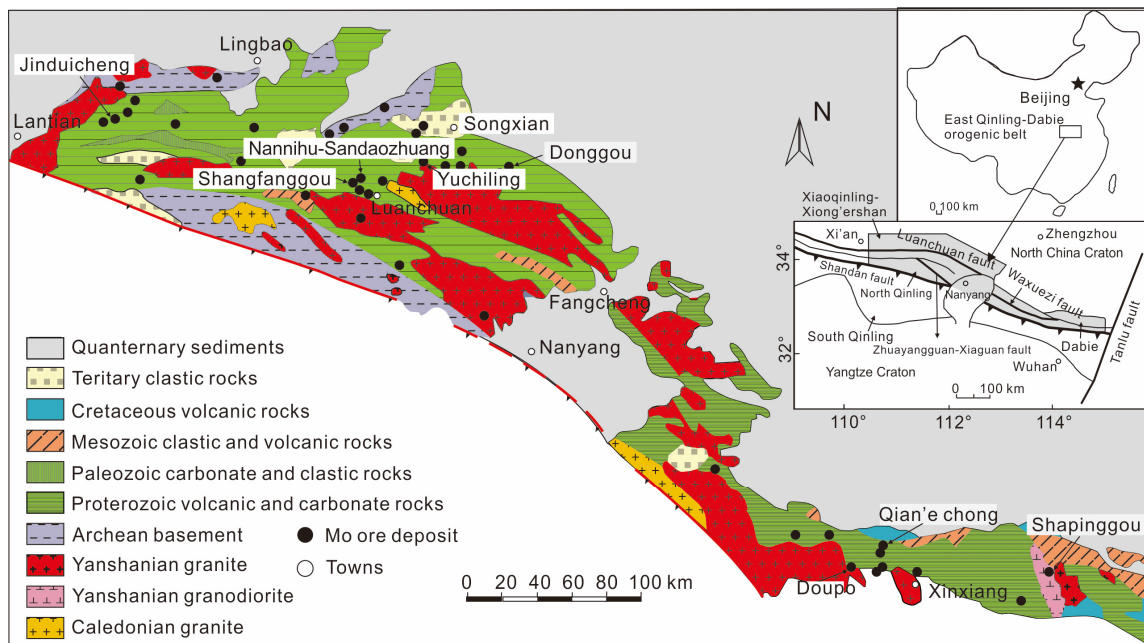


Figure 2. Simplified geology and distribution of Mo deposits in the East Qinling–Dabie Mo mineralization belt (after [68]).

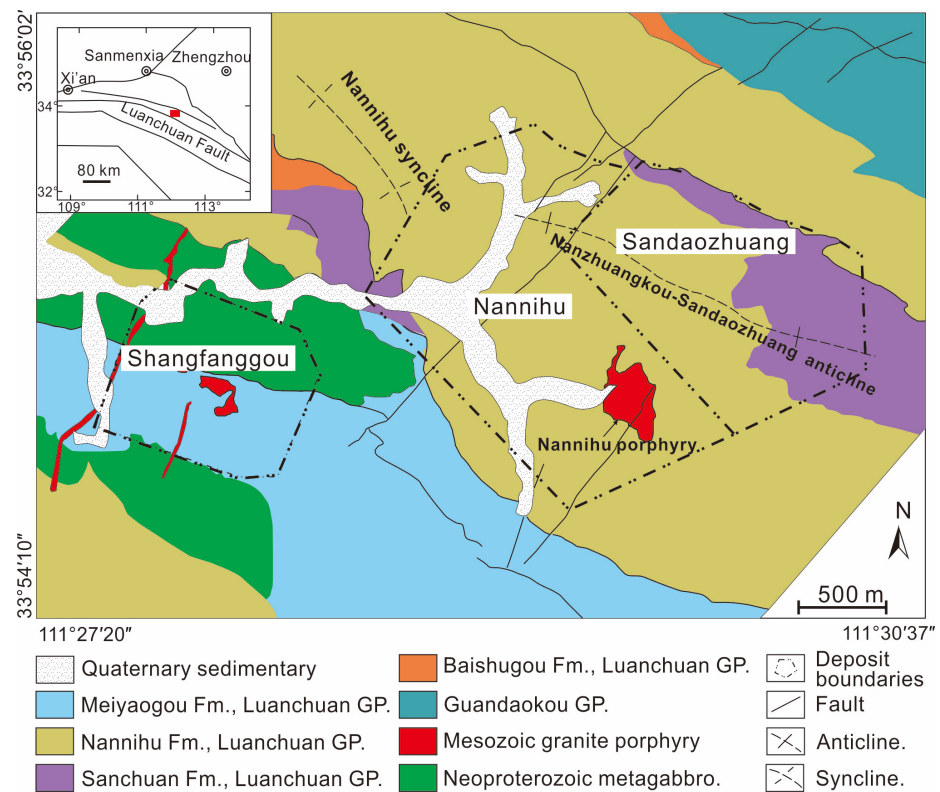


Figure 3. Geological map of the Luanchuan Mo field (after [68]).

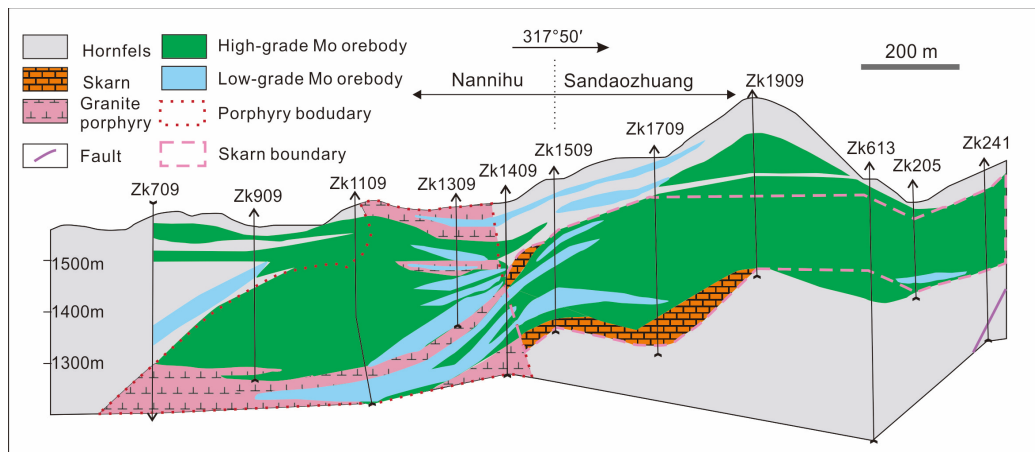


Figure 4. Geological section along the No. 9 exploration line in the Nannihu-Sandaozhuang W-Mo deposit (after [53]).

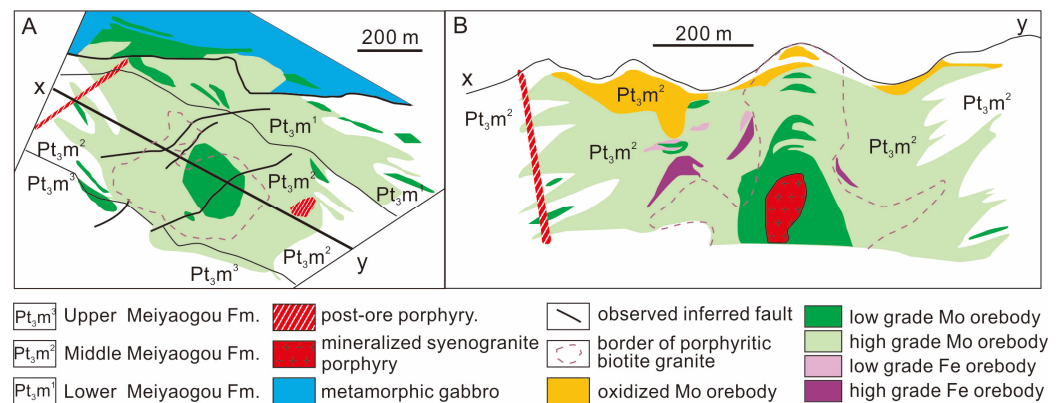


Figure 5. Geological map at the 1132 m level (A) and cross-section (B) of the Shangfanggou porphyry Mo deposit (after [27]).

The mineralization process can be divided into four stages: (1) stage I, characterized by silicification, potassium and skarn alteration, with small amounts of magnetite and molybdenite; (2) stage II, the main Mo mineralization stage, characterized by intense silicification and sericitization, containing numerous quartz–K-feldspar–molybdenite veins, quartz–molybdenite veins and quartz–sulfide veins; (3) stage III, characterized by poly-metallic sulfide mineralization, dominated by pyrite veins and quartz–sulfide–carbonate veins; and (4) stage IV, characterized by carbonate veins, quartz–carbonate veins and carbonate–fluorite veins, with almost no sulfides. Mineralization assemblages indicate a gradual decrease followed by an increase in the ore-forming system’s oxygen fugacity from the early to late stage.

The calcite in the Nannihu-Sandaozhuang-Shangfanggou Mo (W) porphyry-skarn deposits exhibits extremely low $\delta^{13}C_{V-PDB}$ values (-9.1‰ to -1.6‰ , mean of -5.9‰), which are significantly different from those of the sedimentary marine carbonates in the Sanchuan Formation. This indicates that some carbon-enriched ^{12}C originates from the carbonaceous rocks surrounding the deposits [53,55,69]. During ore formation, the $\delta^{13}C_{V-PDB}$ values of calcite gradually increase, but its $\delta^{18}O_{V-SMOW}$ values gradually decrease [69]. This suggests a decrease in the addition of CH_4 from the carbonaceous surrounding rocks and an increase in the amount of atmospheric precipitation from the early to late stages, which is consistent with the redox state transformation revealed by mineral assemblages. During the mineralization process, carbonaceous surrounding rocks undergo thermal decomposition or react with hydrothermal fluids to produce CH_4 and CO_2 , resulting in an increased CO_2

concentration and a decreased oxygen fugacity in the ore-forming solutions. Sulfate is reduced to sulfide and combines with Mo^{2+} and other metallic elements to form much sulfide precipitation.

2.2. Shapinggou Porphyry Mo Deposit

The Shapinggou porphyry Mo deposit is in the eastern Dabie orogenic belt, with a total proven reserve of 1.6 Mt Mo metal, averaging a grade of 0.125% Mo. The main sedimentary layers exposed in this area are metavolcanic and metasedimentary rocks of the Neoproterozoic Luzhenguan Group, which is composed of biotite plagioclase gneiss, monzonite gneiss, plagioclase amphibolite gneiss, variolite, marble, muscovite schists, and graphite schists. Due to intense Yanshanian magmatic activity, the Luzhenguan Group is preserved as residual and captured bodies in the western and northern areas of this region (Figure 6) [70–72]. Graphite-mica-quartz schist and graphite-andalusite phyllite in the Xianrenchong Formation of the Luzhenguan Group are enriched to form graphite deposits in Jinzhai-Tiechongxiang-Zaohe (Figure 1A,B). Faults control the cylindrical orebodies, which are mainly hosted in the contact zone between the porphyry granite and the surrounding diorite, with scattered orebodies distributed around the area. Lead-zinc and fluorite ores are abundant and encircle the Shapinggou deposit. The deposit shows well-defined alteration zoning of K (Na)-feldspar-quartz, pyrite-sericite-quartz, and chlorite-carbonate from the center granite porphyry outward. The mineralization process can be divided into four stages: (I) K (Na)-feldspar-quartz-magnetite/hematite stage; (II) quartz-K-feldspar-molybdenite stage, which is the main mineralization stage of molybdenite, dominated by quartz-(pyrite)-molybdenite veins in the contact zone between porphyry and surrounding rocks; (III) pyrite-sericite stage, characterized by abundant pyrite, sericitization, and silicification, with weak Mo mineralization; and (IV) quartz-fluorite-gypsum stage, characterized by abundant quartz-fluorite and gypsum veins (Figure 7). The above mineral assemblages indicate that the oxidation state of the mineralizing system gradually decreases from the early stage to the main ore-forming stage, and then increases in the late stage.

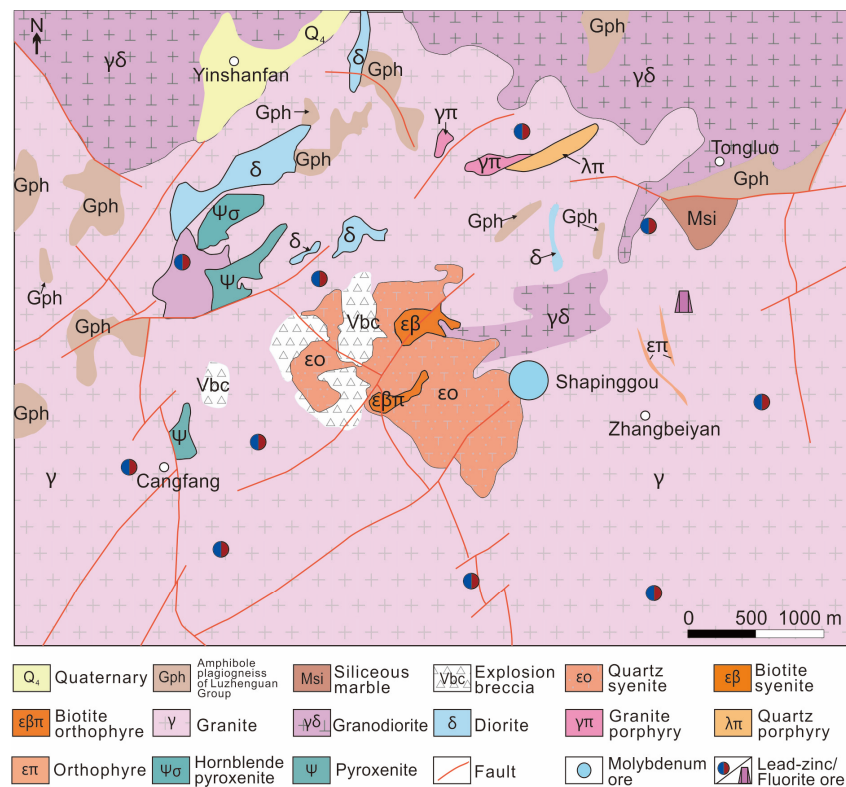


Figure 6. Geological map of the Shapinggou Mo deposit (modified from [71]).

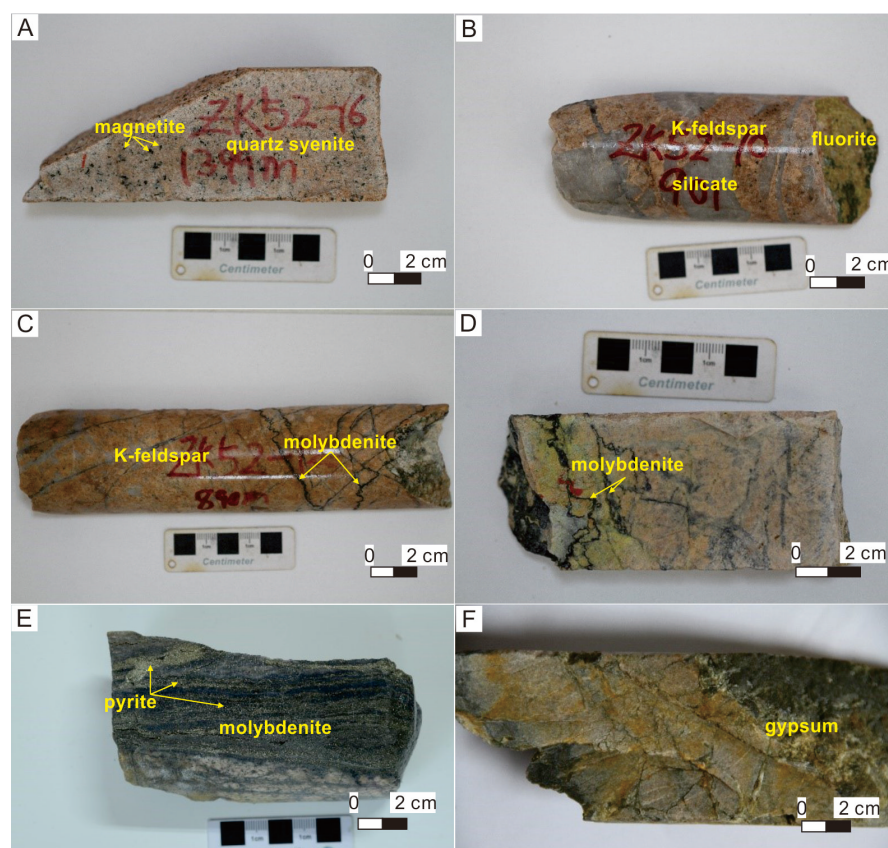


Figure 7. Photographs of geological features in the Shapinggou porphyry Mo deposit. (A) Primitive magnetite developed in fresh quartz syenite from deep deposits. (B) Potassium alteration, silicification, and fluoritization from the early to late stages. (C) Potassium alteration and vein of molybdenite mineralization. (D) Sawtooth-shaped molybdenite filled in the fissures. (E) Later disseminated pyrite replaced earlier molybdenite. (F) White gypsum veins filled in the fractures in the late stage.

Due to the regional crustal uplift and erosion, the argillization, propylitic alteration zone, and vein-type Pb–Zn orebodies above the granite porphyry have been completely eroded, whereas the alteration zones and orebodies on both sides of the granite porphyry are preserved. The granite porphyry is now preserved approximately 400 m underground, with its top surface formed at a depth of approximately 2.2 km, and the erosion zone is estimated to be 1.8 km, making the main orebodies approach the surface. Most carbonaceous layers in the Luzhenguan Group in the Shapinggou Mo deposit may have been eroded and distributed sporadically as remnants inside and outside the field.

2.3. Yuchiling Porphyry Mo Deposit

The Yuchiling deposit is a giant porphyry Mo deposit located west of the East Qinling–Dabie Mo mineralization belt in Henan Province, China. The main lithostratigraphic units are the Taihua Supergroup (basement) and the Xiong'er Group (cover) (Figure 8) [73]. The Taihua Supergroup, composed of a suite of amphibolite- to granulite-facies metamorphic rocks containing graphite-rich schist, is widely distributed in the Qinling–Dabie metallogenic belt. The carbonaceous sedimentary layers in the Taihua Supergroup, such as the Shuidigou Formation, containing carbonaceous mudstone and limestone, and the Huanchiyu Formation, composed of clastic, argillaceous, carbonaceous dolomitic limestone, and ferrimafic volcanic rocks, have formed graphite deposits in Lushan and Lingbao, respectively [60,61]. The Jidanping Formation and Majiahe Formation of the Xiong'er Group, which are predominantly composed of basaltic andesite, andesite, and dacite, are widely distributed north of the Machaoying Fault.

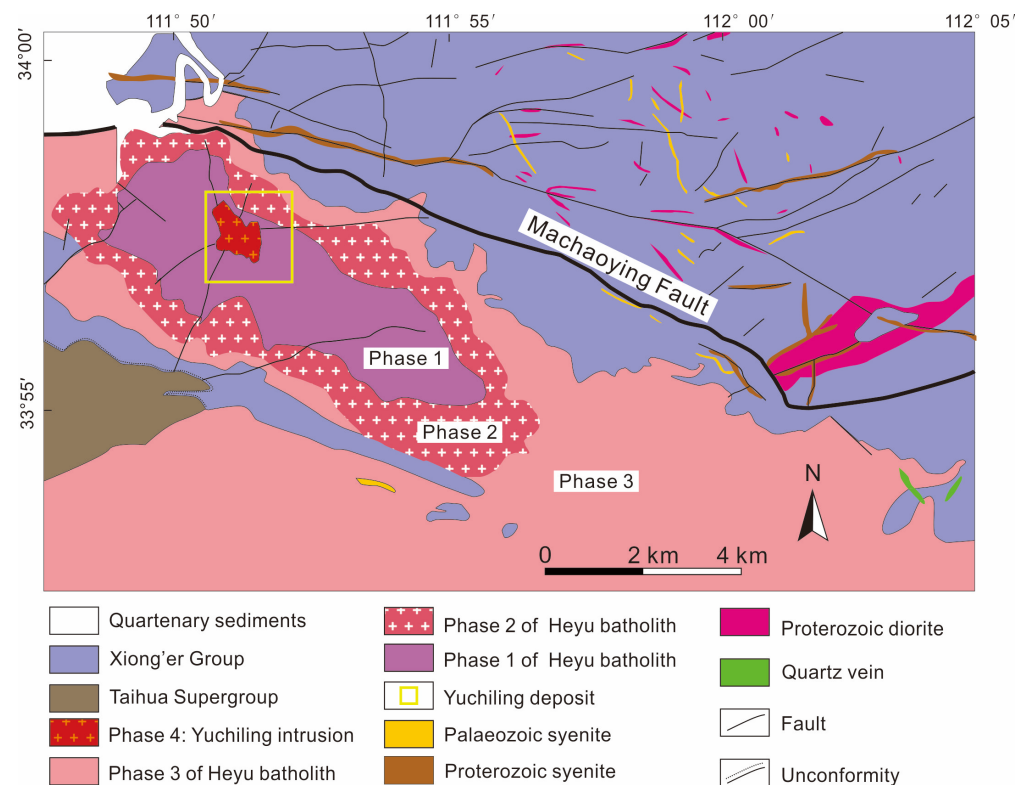


Figure 8. Geological map of the Yuchiling Mo deposit (after [73]).

The Heyu batholith is a concentrically zoned suite consisting of four nested, texturally distinguishable phases. There are breccia pipes genetically associated with Mo mineralization in the granite intrusion, which contain predominant granulite of the Taihua Supergroup and andesite of the Xiong'er Group. The orebody is mainly hosted in the top and bottom of the breccia and in the surrounding granite and fault zones in the central part of the Heyu batholith and occurs as a thick tabular shape with an average thickness of 178.11 m, showing decreasing grades upward [29,74,75]. The ore-forming processes can generally be divided into three stages: (I) molybdenite-K-feldspar stage, with pervasive potassic alteration and weak Mo mineralization. Fluid inclusions in this stage contain gypsum, hematite, and other highly oxidized minerals, indicating a high oxygen fugacity of fluids rich in SO_4^{2-} . (II) The quartz-pyrite-molybdenite stage is characterized by veinlets, net veins, and disseminated molybdenite and pyrite (the main mineralization stage). Fluid inclusions contain less SO_4^{2-} but show the presence of CH_4 , indicating a lower oxygen fugacity than the previous stage; (III) The quartz-fluorite-calcite stage is characterized by pyritic sericitization with weak mineralization. Fluid inclusions contain CH_4 and C_2H_6 , indicating a further decrease in oxygen fugacity during this stage [28,29].

The Yuchiling deposit contains a shallowly buried orebody spanning from 730 to 190 m in elevation. The deposit displays an outcrop of the orebody and the mineralized porphyry, suggesting that it has undergone extensive tectonic uplift and erosion since its formation. The widespread graphite-bearing phyllite of the Taihua Supergroup and volcanic rocks of the Xionger Group, which existed during the formation of the deposit, have been significantly eroded and now exist only in the breccia pipes situated in the southwestern and northeastern parts of the mining area. It is possible that the graphite-bearing phyllite of the Taihua Supergroup may have played a role in the formation of the deposit by providing CH_4 as a reductive agent, thereby reducing the oxidized porphyry and efficiently facilitating sulfide precipitation.

2.4. Mt. Emmons Porphyry Mo Deposit

Mt. Emmons lies in the west-central portion of the Colorado (Climax-Henderson) Mo mineralization belt on the eastern coast of the Pacific Ocean. Giant or large Mo deposits, such as the Urad-Henderson, Climax, Mt. Emmons, and Silver Creek deposits, are developed in this belt (Figure 9A). The Mt. Emmons ore field contains two deposits below the Redwell Basin and a third deposit under the Red Lady Basin (Figure 9B). The surrounding sedimentary rocks of the Mancos and Mesaverde Formations consist of dark carbonaceous shale and sandstone beds, which are capped by conglomeratic sandstone beds of the Tertiary Ohio Creek and Wasatch Formations [76]. The granite porphyry stocks intrude the carbonaceous surrounding rocks, forming an altered hornfel contact zone bearing pyrite-pyrrhotite. The black carbonaceous surrounding rocks are altered and discolored, and an innermost 300 m-thick facies of brown hornfels surrounding the stocks grade outward to a 150 m-thick facies of black hornfels [25,77].

The Climax and Urad-Henderson superlarge Mo deposits have geological characteristics and mineralization ages similar to those of the Mt. Emmons deposit. Orebodies occur in the Mesoproterozoic silver plume granite pluton [3,4,78,79]. Previous studies have demonstrated the prevalence of carbonaceous shale, sandstone, mudstone, oil shale, and coal within the Wasatch Formation and the Mesaverde Group in Wyoming and Utah in Colorado [25,62–67]. Technically, the mean recoverable gas resources have been estimated at $7 \times 10^{12} \text{ m}^3$ with primary sources being coal, carbonaceous shale and siltstone in the Mesaverde Group [80]. In this region, dark carbonaceous shale and mudstone serve as the dominant hydrocarbon sources, providing reductive agents and effective water-resisting layers for mineralization. The absence of carbonaceous sedimentary layers from the Wasatch Formation and Mesaverde Group in the Climax and Urad-Henderson Mo deposits may be attributed to regional crustal uplift and erosion.

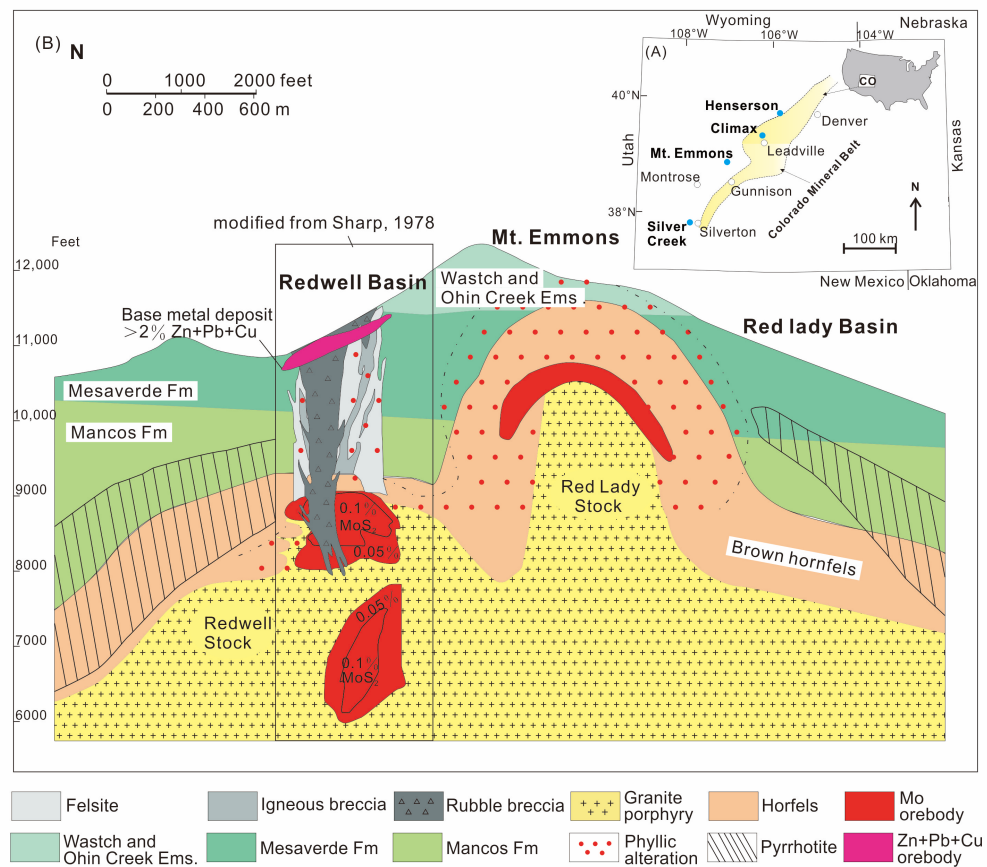


Figure 9. (A) Map of Colorado showing the locations of the Urad–Henderson, Mt. Emmons and Silver Creek porphyry Mo deposits and the outlines of the Colorado Mineral Belt; (B) Schematic

cross-section through the porphyry Mo deposits in the Redwell Basin and Mt. Emmons, Colorado, in America (modified from [40,46,77]). Black carbonaceous sedimentary layers are widespread in porphyry Mo deposits. Due to tectonic uplift and erosion in some areas, the reductive carbonaceous rocks that once covered the Mo deposits have been completely eroded, such as at the Climax and Urad-Henderson porphyry Mo deposits in America [79]. Carbonaceous rocks may remain only at the periphery of the mining area, such as at the Yuchiling porphyry Mo deposit [73], or appear sporadically in the form of remnants inside and outside the mining area, such as at the Shapinggou porphyry Mo deposit [71]. Notably, the development of reductive components such as graphite ores/coal, dark carbonaceous mudstone/limestone, and natural gas nearby indicates that pre-existing carbonaceous surrounding rocks involved in porphyry Mo mineralization may have been eroded in these deposits. Carbonaceous surrounding rocks provide reductive agents for oxidizing ore-forming fluids and promote sulfate reduction to form Mo and other mineral ores, which is an essential factor for forming large high-grade porphyry Mo deposits.

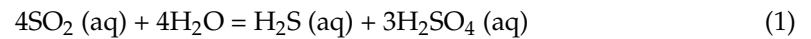
3. Discussion

3.1. Redox State Transformation

High oxygen fugacity magma is a necessary factor for forming porphyry Mo deposits. However, not all oxidized magma can be further metallogenic, as the formation of these deposits not only requires migration of soluble ore-forming materials such as Mo, Cu, and S, but also enrichment of Mo, Cu, and S in the form of sulfide precipitation in the trap location [81]. Sulfur exists mainly as sulfate anions in highly oxidized magma and sulfides in porphyry Mo ores, indicating that the oxidized state of sulfur has undergone significant changes in the mineralization process, which a series of geological phenomena have proven. For example, in Shapinggou porphyry Mo deposits, the Eu/Eu^* and $\text{Ce}^{4+}/\text{Ce}^{3+}$ ratios of zircons in ore-related porphyry are generally high, indicating that the porphyry is highly oxidized [82]. At high temperatures in the early potassium-silicate stage, the Mo mineralization is weak, and the mineral assemblage is characterized by highly oxidized minerals such as magnetite, hematite, and anhydrite, indicating a high oxygen fugacity. This is also proven by magnetite that is rich in fresh mineralized porphyries and hematite daughter minerals in early fluid inclusions. Subsequently, at moderate temperature during the main potassium-quartz-molybdenum-pyrite-sericite stage, highly oxidized minerals such as magnetite and anhydrite are absent, indicating a decrease in oxygen fugacity. In the late stage, chlorite-quartz-fluorite-gypsum-carbonate mineral assemblages appear, indicating an increase in oxygen fugacity [71,72]. In the Nannihu-Sandaozhuang Mo-W deposits, the mineral assemblages are characterized by magnetite and hematite in the early stage, indicating primitive magma with high oxygen fugacity; in the middle stage, fluid inclusions contain reductive components such as CH_4 , H_2S , and CO with precipitation of sulfides, indicating a decrease in oxygen fugacity; in the late stage, there is little reduced gas and weak sulfide mineralization, indicating an increase in oxygen fugacity [22,83]. In the Shangfanggou and Yuchiling Mo deposit, contents vary from magnetite/haematite to reductive gases such as CO , CH_4 , H_2S , and C_2H_6 in the fluid inclusions, showing that oxygen fugacity decreased from the early to the late stage [27,28].

There are three different viewpoints on the causes of the reduction of the highly oxidized ore-forming fluids in porphyry magmatic-hydrothermal systems: (1) magnetite crystallization. Magnetite crystallization may decrease the oxygen fugacity of highly oxidized magma [35,81,84]. Nevertheless, magnetite crystallization cannot reduce magma oxygen fugacity but instead increases residual magma oxygen fugacity in relatively oxidized porphyry magmas [85]. (2) The second cause is SO_2 degassing. SO_2 degassing is considered one of the causes of the redox state transformation in magmatic-hydrothermal systems [86], whereas SO_2 degassing causes $f\text{O}_2$ values of melt to increase rather than decrease in typically sulfur-rich, moderately oxidized arc magmas [85]. Moreover, sulfur mainly exists in the form of SO_4^{2-} in highly oxidized magmas, and SO_2 is a volatile gas that constantly reacts with other components until it reaches a stable state. Therefore, SO_2 may

be an intermediate product of SO_4^{2-} reduction or S^{2-} oxidation [42]. (3) The third cause is the reaction of SO_2 disproportionation. The traditional view is that evolved hydrothermal fluids have high-oxidation levels similar to those of primitive magma. When they are cooled to 450 °C, as both an oxidizer and a reducing agent, the SO_2 in the hydrothermal fluids is disproportionated to form H_2S and H_2SO_4 (Formula (1)), which then combine with metals such as Fe, Mo, and Ca to form sulfides and anhydrite precipitation, respectively [85,87–89]. However, suppose that the disproportionation of SO_2 is the primary mechanism for providing reduced sulfur to the metallogenic system. In that case, much more anhydrite will be formed than sulfides, which is inconsistent with field observations.



Therefore, the three mechanisms mentioned above may contribute to the redox state transformation of the ore-forming system. Nevertheless, they may not be the primary process for large-scale, high-grade porphyry Mo deposit formation.

3.2. Involvement of Carbonaceous Surrounding Rocks

Carbonaceous surrounding rocks have played a significant role in mineralizing porphyry Mo deposits, although their contribution has been neglected in previous research. Specific surrounding rocks obviously control the distribution and grade of ores in many porphyry Mo (Cu) deposits globally, of which ores occur directly in the surrounding rocks or contact zones between porphyry and surrounding rocks, such as the Mt. Emmons Mo deposit in America [25], El Teniente Cu-Mo deposit in Chile [57,58], Oyu Tolgoi Cu-Au-Mo deposit in Mongolia [90] and Nannihu-Sandaozhuang-Shangfanggou porphyry-skarn Mo-W deposits in China [51]. Reductive components are variable in the surrounding rocks and can be divided mainly into reductive Fe-rich volcanic rocks and carbonaceous surrounding rocks.

(1) For Reductive Fe-rich volcanic rocks, SO_4^{2-} from highly oxidized mineralized magma-hydrothermal fluids is reduced to S^{2-} by Fe^{2+} from surrounding Fe-rich volcanic rocks, while Fe^{2+} is oxidized to form magnetite/hematite, and S^{2-} combines with residual Fe^{2+} and Mo^{4+} to form pyrite and Mo ores (Formula (2)) [91–94]. Reductive Fe-rich volcanic rocks are widely distributed in many porphyry Cu-Mo deposits across the world, such as ferrimafic andesite in porphyry Cu-Mo deposits in South America [57,58], the gabbro-diorite-andesite complex in the El Teniente porphyry Cu-Mo deposits in Chile [56,59], and a series of tholeiitic basalts in the Oyu Tolgoi porphyry Cu-Mo deposit in Mongolia [90]. The porphyry Mo deposits in the Qinling-Dabie Mo belt in China are also hosted in the andesite-basaltic surrounding rocks, such as the Jinduicheng and the Donggou Mo deposits, wherein ores are situated in the contact zones between the mineralized granodiorite porphyries and the andesite-basalts of the Xionger Group [68,95]. These Fe-rich volcanic rocks provide a large amount of Fe^{2+} as a reductive agent for the oxidized porphyry metallogenic system, promoting the rapid reduction of SO_4^{2-} and efficient enrichment and precipitation of Fe, Mo, Cu and other metal elements, forming high-grade Mo ores in the contact zone between the metallogenic porphyry and the Fe-rich surrounding rocks, with excess SO_4^{2-} forming gypsum and other sulfates.



(2) Reductive carbonaceous surrounding rocks. Reductive carbonaceous surrounding rocks represent another essential reductive component in mineralizing porphyry deposits. It is widely accepted that most porphyry Cu deposits form from highly oxidized ore fluids. However, several otherwise typical porphyry Cu deposits exhibit clear evidence of formation from relatively reduced ore fluids. These “reduced” porphyry Cu deposits lack primary hematite, magnetite, and sulfate minerals (i.e., anhydrite) but contain abundant magmatic pyrrhotite and commonly have carbonic-rich ore fluids with substantial CH_4 [96]. It has been proposed that, similar to oxidized porphyry copper deposits, the original parent magma of these “reduced” porphyry Cu deposits was oxidized but reduced after assimilation with graphitic layers during magmatic stage [81,96,97]. Recent studies have

also indicated that some porphyry Mo deposits are reduced, and these deposits are called “reduced” porphyry Mo deposits, such as the Suyunhe, Hongyuan, and Baishan Mo deposits in Xinjiang Province, China [98]. In fact, the influence of carbonaceous surrounding rocks on porphyry mineralization is not limited to the magmatic stage. Carbonaceous sedimentary layers are widely distributed in porphyry Mo deposits, and the involvement of reduced components occurs more commonly during the hydrothermal stage, which will be discussed in Section 3.4.

3.3. CH₄ as an Important Reductive Component

Carbonaceous surrounding rocks provide a porphyry mineralization system with carbonaceous reductive agents and gas reductive agents such as CH₄. CH₄ is produced by the thermal decomposition of organic matter or carbonaceous reaction with hydrothermal fluids (Formula (3)) [99,100]. It is the main reductive gas component found in the fluid inclusions of porphyry Mo deposits. For example, reductive gases such as CH₄, CO, H₂S, and C₂H₆ can be observed in the fluid inclusions of the main mineralization stage in the Nannihu-Shangfanggou and Shapinggou porphyry Mo deposits (Figure 10) [27,83,101]. Much recoverable natural gas have been estimated in the Mesaverde Group and Wasatch Formation in the Climax, Mt. Emmons, and Urad-Henderson deposits, indicating the involvement of CH₄ in the mineralization process.

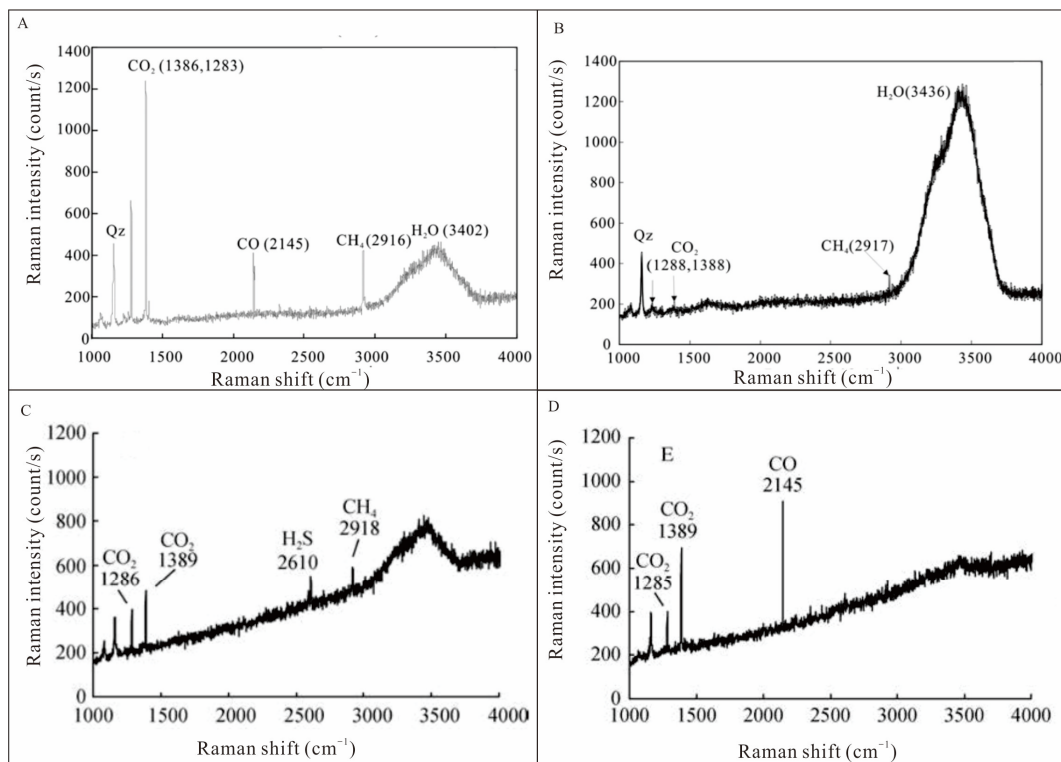
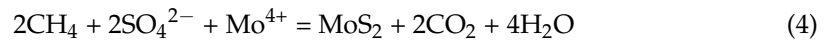


Figure 10. Laser Raman spectra of the fluid inclusions of the porphyry Mo deposits. (A,B). Reductive components such as CH₄ and CO of fluid inclusions in quartz of the Shangfanggou deposit [27]. (C,D). Gas components such as CH₄, H₂S, and CO of C-type inclusions of the Nannihu-Sandaozhuang Mo deposits [83].

As a highly reductive gas component, CH₄ can rapidly migrate over long distances, permeating the ore-forming system along structural fractures without direct contact between the intrusion and carbonaceous surrounding rocks. During mineralization, reductive gases such as CH₄ are produced through the thermal decomposition of organic matter or

by carbonaceous reactions with hydrothermal fluids. By diffusion into the ore-forming porphyry, CH_4 mixed with the oxidized fluids reduces SO_4^{2-} to form S^{2-} . The S^{2-} then combines with Mo, Fe, and Cu to precipitate as Mo ores and other sulfides. Simultaneously, CH_4 undergoes oxidation to produce substantial CO_2 (Formula (4)), as evidenced by porphyritic alteration in the surrounding rocks in the field.



The $\delta^{13}\text{C}_{\text{V-PDB}}$ values of calcite range from -9.1% to -1.6% , with an average of -5.9% in the Nannihu-Sandaozhuang-Shangfanggou porphyry-skarn W-Mo deposits [53,55,69]. In the Shapinggou Mo deposit, the $\delta^{13}\text{C}_{\text{V-PDB}}$ values of calcite range from -2.5% to -1.9% , with an average of -2.3% , and the $\delta^{13}\text{C}_{\text{V-PDB}}$ values of fluid inclusions in quartz veins containing molybdenite are -4.9% , similar to the $\delta^{13}\text{C}_{\text{V-PDB}}$ values of calcite in the Nannihu-Sandaozhuang-Shangfanggou Mo deposits and significantly different from those in marine sedimentary carbonate rocks ($\delta^{13}\text{C}_{\text{V-PDB}} = 2.0\%$ – 2.3%) (Figure 11). The Yingshuisi Pb–Zn deposit hosted in the Xianrenchong Formation of the Luzhenguan Group and the Shapinggou Mo–Pb–Zn deposit are part of the same mineralization system [102,103]. The $\delta^{13}\text{C}_{\text{V-PDB}}$ values of the quartz fluid inclusions in the Yingshuisi Pb–Zn deposit are low (-25.8% to -9.2% , mean of -17.7%) [104], and they are significantly different from the $\delta^{13}\text{C}_{\text{V-PDB}}$ values of the primitive magma and the marine sedimentary carbonates but similar to those of the organic matter, indicating that the Xianrenchong Formation of the Luzhenguan Group that was enriched in graphite provided reducing agents such as CH_4 for the ore-forming system. These results provide reliable evidence for the involvement of the carbonaceous surrounding rocks in the porphyry mineralization.

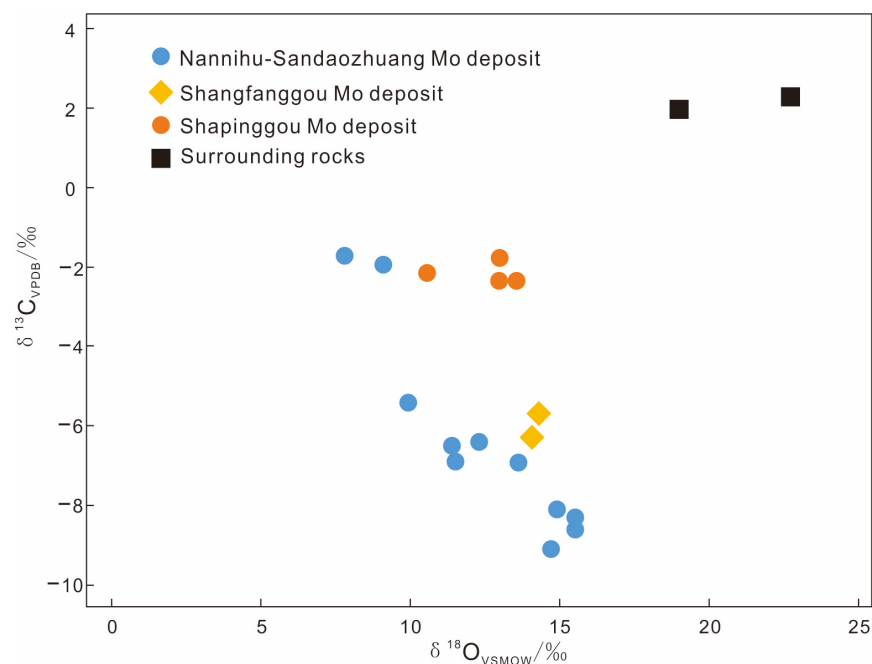


Figure 11. Carbon and oxygen isotopic compositions of calcite from the Nannihu-Sandaozhuang-Shangfanggou porphyry W-Mo deposits, the Shapinggou Mo deposit, and surrounding marine carbonate (data are from [53,55,69] and this study and listed in Table S1).

In summary, carbonaceous surrounding rocks are important for porphyry mineralization, and CH_4 and other reductive gas components are ideal reductive agents for oxidized porphyry mineralization systems.

3.4. Stage of Involvement of Carbonaceous Surrounding Rocks

The involvement of reductive components in the carbonaceous surrounding rocks mainly occurs in the hydrothermal stage rather than in the magmatic stage. There are two cases of involvement of the reductive components during the ore-forming magmatic emplacement process.

The highly oxidized ore-forming porphyry may have assimilated and mixed with the carbonaceous surrounding rocks in the magma chamber during the upwelling process, producing so-called reductive porphyry [96]. The involvement of the reductive components in the magmatic stage can reduce SO_4^{2-} into metal sulfide precipitation and disperse ore-forming materials. This is unfavorable for the immigration of Mo, S, and other ore-forming materials in the melt, rarely forming giant/large porphyry Mo deposits [34].

Second, the involvement of the reductive components in the carbonaceous surrounding rocks occurs in the hydrothermal stage. This can be further divided into two cases: (a) If the carbonaceous contents in the surrounding rocks are high, a large amount of CH_4 with a high concentration can be produced, which diffuses rapidly to the ore-forming system along structural fractures, mixing with oxidized ore-forming fluids. This leads to the reduction of SO_4^{2-} in the hydrothermal fluids, forming sulfide precipitation mainly in the porphyry intrusion, such as in the Shapinggou [71] and Yuchiling [74,75] porphyry Mo deposits. (b) Suppose the carbonaceous contents in the surrounding rocks are low, and CH_4 is insufficient to reduce the sulfate in the hydrothermal fluids, then, in that case, the remaining oxidized ore-forming hydrothermal fluids migrate to the surrounding rocks along the structural fractures and react with reductive agents such as C and CH_4 in the carbonaceous surrounding rocks to form sulfide precipitates. The orebodies mainly occur in the contact zone between the porphyry and the carbonaceous surrounding rocks, such as in the Nannihu-Sandaozhuang-Shangfanggou porphyry Mo deposits [27,55]. Therefore, when CH_4 is used as a reductive agent, orebodies may occur in the surrounding rock, the contact zone between the porphyry intrusion and the surrounding rock, and within the porphyry intrusion itself.

4. Conclusions

(1) Black carbonaceous sedimentary layers are widely developed in giant/large porphyry Mo deposits worldwide. These sedimentary layers have been eroded or partially removed within the deposits due to intrusive rocks or tectonic uplift but may still be preserved in the periphery of the deposits. The high oxygen fugacity of magma is necessary for the mineralization of porphyry Mo deposits. The involvement of the reductive components from the carbonaceous surrounding rocks is the key to triggering the transformation of the ore-forming system's redox state and mineral precipitation.

(2) CH_4 is an important reductive agent that carbonaceous surrounding rocks provide to the porphyry ore-forming system. The CH_4 diffuses into the ore-forming system along the structural fractures and can reduce the ore-forming system without direct contact between the intrusion and the carbonaceous surrounding rocks.

(3) The high oxygen fugacities of the magma and the carbonaceous surrounding rocks/Fe-rich volcanic rocks are effective indicators for evaluating the potential mineralization of porphyry Mo deposits.

Supplementary Materials: The following are available online at <https://www.mdpi.com/article/10.3390/min13070951/s1>, Table S1: Carbon and oxygen isotopic compositions of calcite from the Nannihu-Sandaozhuang-Shangfanggou porphyry W-Mo deposits, the Shapinggou Mo deposit, and surrounding marine carbonate.

Author Contributions: Data curation, D.G. and Y.L.; Formal analysis, C.F.; Funding acquisition, Y.L. and C.D.; Writing—original draft, D.G.; Writing—review and editing, Y.L., C.D. and P.S. All authors have read and agreed to the published version of the manuscript.

Funding: This study was jointly supported by the National Natural Science Foundation of China (No. 41973022, 41627802 and 42172102) and Central Public-interest Scientific Institution Basal Research Fund (No. KK2015).

Data Availability Statement: Data openly available in a public repository. Supplementary Materials Table S1: Carbon and oxygen isotopic compositions of calcite from the Nannihu-Sandaozhuang-Shangfanggou porphyry W-Mo deposits, the Shapinggou Mo deposit, and surrounding marine carbonate.

Acknowledgments: We gratefully thank two anonymous reviewers for their helpful comments and insightful reviews, which have greatly improved the manuscript.

Conflicts of Interest: The authors declare no conflict of interest.

References

1. U.S. Geological Survey. *USGS Mineral Commodity Summaries 2023*; U.S. Geological Survey: Reston, VA, USA, 2023.
2. Sillitoe, R.H. Types of porphyry molybdenum deposits. *Min. Mag.* **1980**, *142*, 550–553.
3. Seedorff, E.; Marco, T.E. Henderson Porphyry Molybdenum System, Colorado: I. Sequence and Abundance of Hydrothermal Mineral Assemblages, Flow Paths of Evolving Fluids, and Evolutionary Style. *Econ. Geol. Bull. Soc. Econ. Geol.* **2004**, *99*, 3–37. [[CrossRef](#)] [[PubMed](#)]
4. Seedorff, E.; Marco, T.E. Henderson Porphyry Molybdenum System, Colorado: II. Decoupling of Introduction and Deposition of Metals during Geochemical Evolution of Hydrothermal Fluids. *Econ. Geol. Bull. Soc. Econ. Geol.* **2004**, *99*, 39–72. [[CrossRef](#)]
5. Ludington, S.; Plumlee, G.S. *Climax-Type Porphyry Molybdenum Deposits*; US Geological Survey Open-File Report; U.S. Geological Survey: Reston, VA, USA, 2009; Volume 1215.
6. Heintze, L. Geology and Geochemistry of the Porphyry Stockwork Molybdenum Deposit at Tamboras, La Negra Zone (Peru). *Econ. Geol.* **1985**, *80*, 2019–2027. [[CrossRef](#)]
7. Linnen, R.L.; Williams-Jones, A.E. Evolution of Aqueous-Carbonic Fluids during Contact Metamorphism, Wall-Rock Alteration, and Molybdenite Deposition at Trout Lake, British Columbia. *Econ. Geol.* **1990**, *85*, 1840–1856. [[CrossRef](#)]
8. Carten, R.B.; White, W.H.; Stein, H.J. *High-Grade Granite-Related Molybdenum Systems: Classification and Origin*; Special Paper; Geological Association of Canada: St. John's, NL, Canada, 1993; Volume 40, pp. 521–554.
9. Selby, D.; Nesbitt, B.E.; Muehlenbachs, K.; Prochaska, W. Hydrothermal Alteration and Fluid Chemistry of the Endako Porphyry Molybdenum Deposit, British Columbia. *Econ. Geol.* **2000**, *95*, 183–202. [[CrossRef](#)]
10. Lawley, C.J.M.; Richards, J.P.; Anderson, R.G.; Creaser, R.A.; Heaman, L.M. Geochronology and Geochemistry of the MAX Porphyry Mo Deposit and Its Relationship to Pb-Zn-Ag Mineralization, Kootenay Arc, Southeastern British Columbia, Canada. *Econ. Geol.* **2010**, *105*, 1113–1142. [[CrossRef](#)]
11. Tang, J.X.; Chen, Y.C.; Wang, D.H.; Wang, C.H.; Xu, Y.p.; Qu, W.J.; Huang, W.; Huang, Y. Re-Os Dating of Molybdenite from the Sharang Porphyry Molybdenum Deposit in Gongbógyamda County, Tibet and Its Geological Significance. *Acta Geol. Sin.* **2009**, *5*, 698–704.
12. Liu, J.; Mao, J.W.; Wu, G.; Wang, F.; Luo, D.F.; Hu, Y.Q. Zircon U-Pb and molybdenite Re-Os dating of the Chalukou porphyry Mo deposit in the northern Great Xing'an Range, China and its geological significance. *J. Asian Earth Sci.* **2014**, *79*, 696–709. [[CrossRef](#)]
13. Liu, Y.H.; Ma, R.; Chen, Z.Y.; Gan, Y.Y.; He, F.; Li, X.Z.; Quan, Z.X.; Zhao, Q.X.; Amu, G.L. Geological characteristics and prospecting indicator of Caosiyao Mo deposit, Inner Mongolia. *Glob. Geol.* **2014**, *2*, 426–432.
14. Wang, G.R.; Wu, G.; Wu, H.; Liu, J.; Li, X.Z.; Xu, L.Q.; Zhang, T.; Quan, Z.X. Fluid inclusion and hydrogen-oxygen isotope study of Caosiyao superlarge porphyry molybdenum deposit in Xinghe County, central Inner Mongolia. *Miner. Depos.* **2014**, *6*, 1213–1232.
15. Li, H.; Sun, H.S.; Wu, J.H.; Evans, N.J.; Xi, X.S.; Peng, N.L.; Cao, J.Y.; Gabo-Ratio, J.A.S. Re-Os and U-Pb geochronology of the Shazigou Mo polymetallic ore field, Inner Mongolia: Implications for Permian-Triassic mineralization at the northern margin of the North China Craton. *Ore Geol. Rev.* **2017**, *83*, 287–299. [[CrossRef](#)]
16. Sun, H.S.; Li, H.; Danišik, M.; Xia, Q.L.; Jiang, C.L.; Wu, P.; Yang, H.; Fan, Q.R.; Zhu, D.S. U-Pb and Re-Os geochronology and geochemistry of the Donggebi Mo deposit, Eastern Tianshan, NW China: Insights into mineralization and tectonic setting. *Ore Geol. Rev.* **2017**, *86*, 584–599. [[CrossRef](#)]
17. Liao, M.Q.; Lai, Y.; Zhou, Y.T.; Shu, Q.H. Zircon U-Pb Dating and Geochemical Analysis of Ore-Bearing Intrusions of Dasuji Porphyry Mo Deposit. *Acta Sci. Nat. Univ. Pekin.* **2018**, *54*, 763–780.
18. Xue, Q.Q.; Zhang, L.P.; Chen, S.; Guo, K.; Li, T.; Han, Z.; Sun, W.D. Tracing black shales in the source of a porphyry Mo deposit using molybdenum isotopes. *Geology* **2023**, *51*, 688–692. [[CrossRef](#)]
19. Li, N.; Chen, Y.J.; Zhang, H.; Zhao, T.P.; Deng, X.H.; Wang, Y.; Ni, Z.Y. Molybdenum deposits in East Qinling. *Earth Sci. Front.* **2007**, *14*, 186–198.
20. Chen, Y.J.; Li, N. Nature of ore-fluids of intracontinental intrusion-related hypothermal deposits and its difference from those in island arcs. *Acta Petrol. Sin.* **2009**, *25*, 2477–2508.
21. Li, C.Y.; Wang, F.Y.; Hao, X.L.; Ding, X.; Zhang, H.; Ling, M.X.; Zhou, J.B.; Li, Y.L.; Fan, W.-M.; Sun, W.-D. Formation of the World's Largest Molybdenum Metallogenic Belt: A Plate-Tectonic Perspective on the Qinling Molybdenum Deposits. *Int. Geol. Rev.* **2012**, *54*, 1093–1112. [[CrossRef](#)]

22. Chen, Y.J.; Li, N.; Deng, X.H. *Molybdenum Mineralization in Qinling Orogeny*; Science Press: Beijing, China, 2020.
23. Liu, Q.; Li, H.; Shao, Y.; Bala Girei, M.; Jiang, W.; Yuan, H.; Zhang, X. Age, Genesis, and Tectonic Setting of the Qiushuwan Cu–Mo Deposit in East Qinling (Central China): Constraints from Sr–Nd–Hf Isotopes, Zircon U–Pb and Molybdenite Re–Os Dating. *Ore Geol. Rev.* **2021**, *132*, 103998. [[CrossRef](#)]
24. Roedder, E. Fluid Inclusion Studies on the Porphyry-Type Ore Deposits at Bingham, Utah, Butte, Montana, and Climax, Colorado. *Econ. Geol.* **1971**, *66*, 98–118. [[CrossRef](#)]
25. Thomas, J.A.; Galey, J.T. Exploration and Geology of the Mt. Emmons Molybdenite Deposits, Gunnison County, Colorado. *Econ. Geol.* **1982**, *77*, 1085–1104. [[CrossRef](#)]
26. Yang, Y.F.; Li, N.; Ni, Z.Y. Fluid inclusion study of the Jinduicheng porphyry Mo deposit, Hua country, Shanxi province. *Acta Petrol. Sin.* **2009**, *25*, 2983–2993.
27. Yang, Y.; Chen, Y.J.; Zhang, J.; Zhang, C. Ore Geology, Fluid Inclusions and Four-Stage Hydrothermal Mineralization of the Shangfanggou Giant Mo–Fe Deposit in Eastern Qinling, Central China. *Ore Geol. Rev.* **2013**, *55*, 146–161. [[CrossRef](#)]
28. Zhang, J.; Ye, H.S.; Shi, M.C.; Meng, F. Metallogenic process of the Yuchiling Mo deposit in East Qinling: Constraints from fluid inclusions. *Geol. Bull. China* **2013**, *32*, 1113–1128.
29. Zhang, J.; Ye, H.S.; Zhou, K.; Meng, F. Processes of Ore Genesis at the World-Class Yuchiling Molybdenum Deposit, Henan Province, China. *J. Asian Earth Sci.* **2014**, *79*, 666–681. [[CrossRef](#)]
30. Audétat, A. Compositional Evolution and Formation Conditions of Magmas and Fluids Related to Porphyry Mo Mineralization at Climax, Colorado. *J. Petrol.* **2015**, *56*, 1519–1546. [[CrossRef](#)]
31. Ouyang, H.; Caulfield, J.; Mao, J.; Hu, R. Controls on the Formation of Porphyry Mo Deposits: Insights from Porphyry (-Skarn) Mo Deposits in Northeastern China. *Am. Mineral.* **2022**, *107*, 1736–1751. [[CrossRef](#)]
32. Mengason, M.J.; Candela, P.A.; Piccoli, P.M. Molybdenum, Tungsten and Manganese Partitioning in the System Pyrrhotite–Fe–S–O Melt–Rhyolite Melt: Impact of Sulfide Segregation on Arc Magma Evolution. *Geochim. Cosmochim. Acta* **2011**, *75*, 7018–7030. [[CrossRef](#)]
33. Chiaradia, M. Copper enrichment in arc magmas controlled by overriding plate thickness. *Nat. Geosci.* **2014**, *7*, 43–46. [[CrossRef](#)]
34. Gao, Y.; Yang, Y.C.; Han, S.J.; Meng, F. Geochemistry of Zircon and Apatite from the Mo Ore-Forming Granites in the Dabie Mo Belt, East China: Implications for Petrogenesis and Mineralization. *Ore Geol. Rev.* **2020**, *126*, 103733. [[CrossRef](#)]
35. Sun, W.; Huang, R.; Li, H.; Hu, Y.; Zhang, C.; Sun, S.; Zhang, L.; Ding, X.; Li, C.; Zartman, R.E. Porphyry Deposits and Oxidized Magmas. *Ore Geol. Rev.* **2015**, *65*, 97–131. [[CrossRef](#)]
36. Ballard, J.R.; Palin, M.J.; Campbell, I.H. Relative Oxidation States of Magmas Inferred from Ce(IV)/Ce(III) in Zircon: Application to Porphyry Copper Deposits of Northern Chile. *Contrib. Miner. Pet.* **2002**, *144*, 347–364. [[CrossRef](#)]
37. Burnham, A.D.; Berry, A.J. An Experimental Study of Trace Element Partitioning between Zircon and Melt as a Function of Oxygen Fugacity. *Geochim. Cosmochim. Acta* **2012**, *95*, 196–212. [[CrossRef](#)]
38. Muñoz, M.; Charrier, R.; Fanning, C.M.; Maksae, V.; Deckart, K. Zircon trace element and O–Hf isotope analyses of mineralized intrusions from El Teniente ore deposit, Chilean Andes: Constraints on the source and magmatic evolution of porphyry Cu–Mo related magmas. *J. Petrol.* **2012**, *53*, 1091–1122. [[CrossRef](#)]
39. Trail, D.; Bruce Watson, E.; Tailby, N.D. Ce and Eu Anomalies in Zircon as Proxies for the Oxidation State of Magmas. *Geochim. Cosmochim. Acta* **2012**, *97*, 70–87. [[CrossRef](#)]
40. Zhang, D. Chemistry, Mineralogy and Crystallization Conditions of Porphyry Mo-Forming Magmas at Urad–Henderson and Silver Creek, Colorado, USA. *J. Petrol.* **2017**, *58*, 277–296. [[CrossRef](#)]
41. Zhou, T.; Zeng, Q.; Chu, S.; Zhou, L.; Yang, Y. Magmatic Oxygen Fugacities of Porphyry Mo Deposits in the East Xing’an–Mongolian Orogenic Belt (NE China) with Metallogenic Implications. *J. Asian Earth Sci.* **2018**, *165*, 145–159. [[CrossRef](#)]
42. Li, Y.H.; Duan, C.; Zeng, P.S.; Jian, W.; Wan, Q.; Hu, G.-Y.; Zhao, X.-Y.; Wu, X.-P. The Role of Reductive Carbonaceous Strata in the Formation of Porphyry Copper Ores. *Acta Geosci. Sin.* **2020**, *41*, 637–650.
43. Xing, K.; Shu, Q.; Lentz, D.R. Constraints on the Formation of the Giant Daheishan Porphyry Mo Deposit (NE China) from Whole-Rock and Accessory Mineral Geochemistry. *J. Petrol.* **2021**, *62*, egab018. [[CrossRef](#)]
44. Xu, L.L.; Bi, X.W.; Zhang, X.C.; Huang, M.L.; Liu, G. Mantle Contribution to the Generation of the Giant Jinduicheng Porphyry Mo Deposit, Central China: New Insights from Combined in-Situ Element and Isotope Compositions of Zircon and Apatite. *Chem. Geol.* **2023**, *616*, 121238. [[CrossRef](#)]
45. Jiang, Z.; Shang, L.; Guo, H.; Wang, X.; Chen, C.; Zhou, Y. An Experimental Investigation into the Partition of Mo between Aqueous Fluids and Felsic Melts: Implications for the Genesis of Porphyry Mo Ore Deposits. *Ore Geol. Rev.* **2021**, *134*, 104144. [[CrossRef](#)]
46. Audétat, A.; Li, W. The Genesis of Climax-Type Porphyry Mo Deposits: Insights from Fluid Inclusions and Melt Inclusions. *Ore Geol. Rev.* **2017**, *88*, 436–460. [[CrossRef](#)]
47. Ouyang, H.; Mao, J.; Hu, R. Geochemistry and Crystallization Conditions of Magmas Related to Porphyry Mo Mineralization in Northeastern China. *Econ. Geol.* **2020**, *115*, 79–100. [[CrossRef](#)]
48. Ouyang, H.; Mao, J.; Hu, R.; Caulfield, J.; Zhou, Z. Controls on the metal endowment of porphyry Mo deposits: Insights from the Luming porphyry Mo deposit, Northeastern China. *Econ. Geol.* **2021**, *116*, 1711–1735. [[CrossRef](#)]
49. Vigneresse, J.L.; Truche, L.; Richard, A. How Do Metals Escape from Magmas to Form Porphyry-Type Ore Deposits? *Ore Geol. Rev.* **2019**, *105*, 310–336. [[CrossRef](#)]

50. Li, Y.F.; Mao, J.W.; Hu, H.B.; Guo, B.J.; Bai, F.J. Geology, distribution, types and tectonic settings of Mesozoic molybdenum deposits in East Qinling area. *Miner. Depos.* **2005**, *292*–304.
51. Ye, H.S.; Mao, J.W.; Li, Y.F.; Yan, C.H.; Guo, B.J.; Zhao, C.S.; Zheng, R.F.; Chen, L. Characteristics and metallogenic mechanism of Mo W and Pb Zn-Ag deposits in Nannihu ore field western Henan province. *Geoscience* **2006**, *81*, 165–174.
52. Yang, Y.; Zhang, J.; Yang, Y.F.; Shi, Y.X. Characteristics of fluid inclusions and its geological implication of the Shangfanggou Mo deposit in Luanchuan county, Henan province. *Acta Petrol. Sin.* **2009**, *25*, 2563–2574.
53. Xiang, J.F.; Pei, R.F.; Ye, H.S.; Wang, C.Y.; Tian, Z.H. New geochronological data of granites and ores from the Nannihu-Sandaozhuang Mo (W) deposit. *Geol. China* **2012**, *39*, 1778–1789.
54. Yang, Y.F.; Li, N.; Chen, Y.J. Fluid Inclusion Study of the Nannihu Giant Porphyry Mo–W Deposit, Henan Province, China: Implications for the Nature of Porphyry Ore-Fluid Systems Formed in a Continental Collision Setting. *Ore Geol. Rev.* **2012**, *46*, 83–94. [[CrossRef](#)]
55. Yang, Y.; Liu, Z.J.; Deng, X.H. Mineralization Mechanisms in the Shangfanggou Giant Porphyry-Skarn Mo–Fe Deposit of the East Qinling, China: Constraints from H–O–C–S–Pb Isotopes. *Ore Geol. Rev.* **2017**, *81*, 535–547. [[CrossRef](#)]
56. Skewes, M.A.; Holmgren, C.; Stern, C.R. The Donoso Copper-Rich, Tourmaline-Bearing Breccia Pipe in Central Chile: Petrologic, Fluid Inclusion and Stable Isotope Evidence for an Origin from Magmatic Fluids. *Min. Depos.* **2003**, *38*, 2–21. [[CrossRef](#)]
57. Cannell, J.; Cooke, D.R.; Walshe, J.L.; Stein, H. Geology, mineralization, alteration, and structural evolution of the El Teniente porphyry Cu-Mo deposit. In *Economic Geology and the Bulletin of the Society of Economic Geologists*; The Economic Geology Publishing Company: Littleton, CO, USA, 2005; Volume 100, pp. 979–1003.
58. Stern, C.R.; Funk, J.A.; Skewes, M.A.; Arevalo, A. Magmatic anhydrite in plutonic rocks at the El Teniente Cu-Mo deposit, Chile, and the role of sulfur and copper-rich magmas in its formation. *Econ. Geol.* **2007**, *102*, 1335–1344. [[CrossRef](#)]
59. Vry, V.H.; Wilkinson, J.J.; Seguel, J.; Millan, J. Multistage Intrusion, Brecciation, and Veining at El Teniente, Chile: Evolution of a Nested Porphyry System. *Econ. Geol.* **2010**, *105*, 119–153. [[CrossRef](#)]
60. Chen, Y.J.; Fu, S.G.; Hu, S.X. The main element character and its significance of different type greenstone belts in southern margin of North-China platform. *J. Nanjing Univ.* **1988**, *1*, 70–84.
61. Ji, H.Z.; Chen, Y.J.; Zhao, Y.Y. Khondalite series and graphite deposits. *China Non-Met. Miner. Ind.* **1990**, *6*, 9–11.
62. Donnell, J.R. *Tertiary Geology and Oil-Shale Resources of the Piceance Creek Basin between the Colorado and White Rivers, Northwestern Colorado*; U.S. Geological Survey: Bulletin, WA, USA, 1961; pp. 835–891.
63. Roehler, H.W. Vermillion Creek coal bed, high-sulfur, radioactive coal of paludal-lacustrine origin in Wasatch Formation of Vermillion Creek basin, Wyoming and Colorado. *AAPG Bull.* **1979**, *63*, 839.
64. Roehler, H.W.; Martin, P.L. *Geological Investigations of the Vermillion Creek Coal Bed in the Eocene Niland Tongue of the Wasatch Formation, Sweetwater County, Wyoming*; U.S. Geological Survey Professional Papers; U.S. Geological Survey: Denver, CO, USA, 1987; p. 1314.
65. Sanchez, J.D. *Stratigraphic Framework, Coal Zone Correlations, And Depositional Environment of The Upper Cretaceous Blackhawk Formation And Star Point Sandstone in The Scofield And Beaver Creek Areas, Nephi 30' x 60' Quadrangle, Wasatch Plateau Coal Field, Carbon County, Utah. Coal Investigations Map*; U.S. Geological Survey: Reston, VA, USA, 1990.
66. Li, Z.; Schieber, J. Composite Particles in Mudstones: Examples from the Late Cretaceous Tununk Shale Member of the Mancos Shale Formation. *J. Sediment. Res.* **2018**, *88*, 1319–1344. [[CrossRef](#)]
67. Collins, B.A. Geology of the Coal-Bearing Mesaverde Formation (Cretaceous), Coal Basin Area, Pitkin Country, Colorado. Master's Thesis, Colorado School of Mines, Golden, CO, USA, 2020.
68. Mao, J.W.; Pirajno, F.; Xiang, J.F.; Gao, J.J.; Ye, H.S.; Li, Y.F.; Guo, B.J. Mesozoic Molybdenum Deposits in the East Qinling–Dabie Orogenic Belt: Characteristics and Tectonic Settings. *Ore Geol. Rev.* **2011**, *43*, 264–293. [[CrossRef](#)]
69. Liu, X.S.; Wu, C.Y.; Huang, B. Origin and evolution of the hydrothermal system in Nannihu-Sandaozhuang molybdenum (tungsten) ore deposit, Luanchuan country, Henan province. *Geochimica* **1987**, *7*, 199–207. [[CrossRef](#)]
70. Xu, G.; Tang, Z.L.; Jiao, J.G.; Han, X.B.; Zhong, J.X.; Wei, X.; Qiu, G.L. The Comparative Study on Small Intrusion Type Molybdenum Deposits of Shapinggou and Jinduicheng. *Northwestern Geol.* **2012**, *45*, 367–369.
71. Lu, S.M.; Li, J.S.; Ruan, L.S.; Zhao, L.L.; Huang, F.; Wang, B.H.; Zhang, H.D. The characteristics of stable isotope geochemistry of Shapinggou molybdenum deposit, Anhui province. *Geoscience* **2019**, *33*, 262–270. [[CrossRef](#)]
72. Ren, Z.; Zhou, T.-F.; Yuan, F.; Zhang, H.-D. Characteristics of the metallogenic system of the Shapinggou super-large porphyry molybdenum deposit in the Dabie orogenic belt, Anhui Province. *Earth Sci. Front.* **2020**, *27*, 353–372. [[CrossRef](#)]
73. Li, N.; Ulrich, T.; Chen, Y.-J.; Thomsen, T.B.; Pease, V.; Pirajno, F. Fluid Evolution of the Yuchiling Porphyry Mo Deposit, East Qinling, China. *Ore Geol. Rev.* **2012**, *48*, 442–459. [[CrossRef](#)]
74. Li, N.; Chen, Y.J.; Ni, Z.Y.; Hu, H.Z. Characteristics of ore-forming fluids of the Yuchiling porphyry Mo deposit, Songxian country, Henan province, and its geological significance. *Acta Petrol. Sin.* **2009**, *25*, 2509–2522.
75. Zhou, K.; Ye, H.-S.; Mao, J.-W.; Qu, W.-J.; Zhou, S.-F.; Meng, F.; Gao, Y.-L. Geological characteristics and molybdenite Re–Os isotopic dating of Yuchiling porphyry Mo deposit in western Henan Province. *Miner. Depos.* **2009**, *28*, 170–184.
76. Lorenz, J.C.; Nadon, G.C. Braided-River Deposits in A Muddy Depositional Setting: The Molina Member of the Wasatch Formation (Paleogene), West-Central Colorado, U.S.A. *J. Sediment. Res.* **2002**, *72*, 376–385. [[CrossRef](#)]

77. Sharp, J.E. Cave Peak, a Molybdenum-Mineralized Breccia Pipe Complex in Culberson County, Texas. *Econ. Geol.* **1979**, *74*, 517–534. [[CrossRef](#)]
78. Clark, K.F. Stockwork Molybdenum Deposits in the Western Cordillera of North America. *Econ. Geol.* **1972**, *67*, 731–758. [[CrossRef](#)]
79. Wallace, S.R.; MacKenzie, W.B.; Blair, R.G.; Muncaster, N.K. Geology of the Urad and Henderson Molybdenite Deposits, Clear Creek County, Colorado, with a Section on a Comparison of These Deposits with Those at Climax, Colorado. *Econ. Geol.* **1978**, *73*, 325–368. [[CrossRef](#)]
80. Drake, R.M., II; Schenk, C.J.; Mercier, T.J.; Le, P.A.; Finn, T.M.; Johnson, R.C.; Woodall, C.A.; Gaswirth, S.B.; Marra, K.R.; Pitman, J.K.; et al. *Assessment of Undiscovered Continuous Tight-Gas Resources in the Mesaverde Group and Wasatch Formation, Uinta-Piceance Province, Utah and Colorado, 2018*; USGS Fact Sheet; U.S. Geological Survey: Reston, VA, USA, 2019.
81. Wilkinson, J.J. Triggers for the Formation of Porphyry Ore Deposits in Magmatic Arcs. *Nat. Geosci.* **2013**, *6*, 917–925. [[CrossRef](#)]
82. Zhang, H. Geochronology and Metallogenesis of the Shapinggou Giant Porphyry Molybdenum Deposit in the Dabie Orogenic Belt. *Acta Geol. Sin.* **2011**, *85*, 12.
83. Shi, Y.X.; Li, N.; Yang, Y. Ore geology and fluid inclusion geochemistry of the Sandaozhuang Mo-W deposit in Luanchuan county, Henan province. *Acta Petrologica Sin.* **2009**, *25*, 2575–2587.
84. Sun, W.; Liang, H.; Ling, M.; Zhan, M.; Ding, X.; Zhang, H.; Yang, X.; Li, Y.; Ireland, T.R.; Wei, Q. The Link between Reduced Porphyry Copper Deposits and Oxidized Magmas. *Geochim. Cosmochim. Acta* **2013**, *103*, 263–275. [[CrossRef](#)]
85. Richards, J.P. The Oxidation State, and Sulfur and Cu Contents of Arc Magmas: Implications for Metallogeny. *Lithos* **2015**, *233*, 27–45. [[CrossRef](#)]
86. Kelley, K.A.; Cottrell, E. The Influence of Magmatic Differentiation on the Oxidation State of Fe in a Basaltic Arc Magma. *Earth Planet. Sci. Lett.* **2012**, *329–330*, 109–121. [[CrossRef](#)]
87. Kusakabe, M.; Komoda, Y.; Takano, B.; Abiko, T. Sulfur isotopic effects in the disproportionation reaction of sulfur dioxide in hydrothermal fluids: Implications for the $\delta^{34}\text{S}$ variations of dissolved bisulfate and elemental sulfur from active crater lakes. *J. Volcanol. Geotherm. Res.* **2000**, *97*, 287–307. [[CrossRef](#)]
88. Simon, A.C.; Ripley, E.M. The Role of Magmatic Sulfur in the Formation of Ore Deposits. *Rev. Miner. Geochem.* **2011**, *73*, 513–578. [[CrossRef](#)]
89. Hedenquist, J.W.; Taran, Y.A. Modeling the Formation of Advanced Argillic Lithocaps: Volcanic Vapor Condensation Above Porphyry Intrusions. *Econ. Geol.* **2013**, *108*, 1523–1540. [[CrossRef](#)]
90. Perello, J.; Cox, D.; Garamjav, D.; Sanjdorj, S.; Diakov, S.; Schissel, D.; Munkhbat, T.; Oyun, G. Oyu Tolgoi, Mongolia; Siluro-Devonian porphyry Cu-Au-(Mo) and high-sulfidation Cu mineralization with a Cretaceous chalcocite blanket. *Econ. Geol. Bull. Soc. Econ. Geol.* **2001**, *96*, 1407–1428. [[CrossRef](#)]
91. Li, Y.H.; Xie, G.Q.; Duan, C.; Han, D. Effect of sulfate evaporate salt layer over the formation of skarn-type iron ores. *Acta Geol. Sin.* **2013**, *87*, 1324–1334.
92. Li, Y.H.; Duan, C.; Han, D.; Chen, X.W.; Wang, C.L.; Yang, B.Y.; Zhang, C.; Liu, F. Effect of sulfate evaporate salt layer for formation of porphyrite iron ores in the Middle-Lower Yangtze River area. *Acta Petrol. Sin.* **2014**, *30*, 1355–1368.
93. Duan, C.; Li, Y.; Mao, J.; Zhu, Q.; Xie, G.; Wan, Q.; Jian, W.; Hou, K. The Role of Evaporite Layers in the Ore-Forming Processes of Iron Oxide-Apatite and Skarn Fe Deposits: Examples from the Middle-Lower Yangtze River Metallogenic Belt, East China. *Ore Geol. Rev.* **2021**, *138*, 104352. [[CrossRef](#)]
94. Guo, D.; Li, Y.; Duan, C.; Fan, C. Involvement of Evaporite Layers in the Formation of Iron Oxide-Apatite Ore Deposits: Examples from the Luohe Deposit in China and the El Laco Deposit in Chile. *Minerals* **2022**, *12*, 1043. [[CrossRef](#)]
95. Ye, H.S.; Mao, J.W.; Li, Y.F.; Guo, B.J.; Zhang, C.Q.; Liu, J.; Yan, Q.R.; Liu, G.Y. SHRIMP Zircon U-Pb and Molybdenite Re-Os Dating for the Superlarge Donggou Porphyry Mo Deposit in East Qinling, China and Its Geological Implication. *Acta Geol. Sin.* **2006**, *80*, 1078–1088.
96. Rowins, S.M. Reduced Porphyry Copper-Gold Deposits: A New Variation on an Old Theme. *Geology* **2000**, *28*, 491–494. [[CrossRef](#)]
97. Ague, J.J.; Brimhall, G.H. Magmatic Arc Asymmetry and Distribution of Anomalous Plutonic Belts in the Batholiths of California: Effects of Assimilation, Crustal Thickness, and Depth of Crystallization. *Geol. Soc. Am. Bull.* **1988**, *100*, 912–927. [[CrossRef](#)]
98. Cao, C.; Shen, P. Advances and Problems in Study of Porphyry Molybdenum Deposits. *Geol. Rev.* **2018**, *64*, 477–497. [[CrossRef](#)]
99. Andersen, T.; Burke, E.A.J. Methane Inclusions in Shocked Quartz from the Gardnos Impact Breccia, South Norway. *EJM* **1996**, *8*, 927–936. [[CrossRef](#)]
100. Fan, H.-R.; Xie, Y.-H.; Wang, K.-Y.; Wilde, S.A. Methane-Rich Fluid Inclusions in Skarn near the Giant REE-Nb-Fe Deposit at Bayan Obo, Northern China. *Ore Geol. Rev.* **2004**, *25*, 301–309. [[CrossRef](#)]
101. He, J. The Yanshanian Magmatism and Mineralization in Shapinggou Porphyry Mo-Polymetallic Deposit, Jinzhai, Anhui. Ph.D. Thesis, Hefei University of Technology, Hefei, China, 2018.
102. Xu, X.C.; Lou, J.W.; Lu, S.M.; Xie, Q.Q.; Chu, P.L.; Yin, T. Re-Os ages of molybdenum-lead-zinc polymetallic deposits and ^{40}Ar - ^{39}Ar ages of related magmatic rocks in Yinshan area, Jinzhai, Anhui Province. *Miner. Depos.* **2009**, *28*, 621–632.

103. Lu, S.M.; Ruan, L.S.; Zhao, L.L.; Wang, B.H.; Zhang, H.D.; Wang, G.G.; Chen, F. Two Stages of Diagenesis and Metallogenesis of Shapingou Molybdenum-Lead-Zinc Ore Field in Jinzhai Country, Anhui Province. *Acta Geol. Sin.* **2016**, *90*, 1167–1181.
104. Wu, H.R.; Xie, Y.L.; Zhong, R.C.; Wang, Y.; An, W.J. Geology, Fluid Inclusion and Stable Isotopes of the Yinshuisi Zn-Pb Deposit, Jinzhai County, Anhui Province. *Geotecton. Metallog.* **2019**, *43*, 967–990. [[CrossRef](#)]

Disclaimer/Publisher’s Note: The statements, opinions and data contained in all publications are solely those of the individual author(s) and contributor(s) and not of MDPI and/or the editor(s). MDPI and/or the editor(s) disclaim responsibility for any injury to people or property resulting from any ideas, methods, instructions or products referred to in the content.